



UPPSALA
UNIVERSITET

*Digital Comprehensive Summaries of Uppsala Dissertations
from the Faculty of Science and Technology 1849*

Numerical ice sheet modeling

Forward and inverse problems

GONG CHENG



ACTA
UNIVERSITATIS
UPSALIENSIS
UPPSALA
2019

ISSN 1651-6214
ISBN 978-91-513-0738-1
urn:nbn:se:uu:diva-392268

Dissertation presented at Uppsala University to be publicly examined in ITC 2446, Ångströmlaboratoriet, Lägerhyddsvägen 2, Uppsala, Friday, 18 October 2019 at 10:15 for the degree of Doctor of Philosophy. The examination will be conducted in English. Faculty examiner: PhD, Principal Member of Technical Staff Irina Tezaur (Sandia National Laboratories in Livermore, CA, USA).

Abstract

Cheng, G. 2019. Numerical ice sheet modeling. Forward and inverse problems. *Digital Comprehensive Summaries of Uppsala Dissertations from the Faculty of Science and Technology* 1849. 43 pp. Uppsala: Acta Universitatis Upsaliensis. ISBN 978-91-513-0738-1.

Ice sheets have strong influence on the climate system. Numerical simulation provides a mathematical tool to study the ice dynamics in the past and to predict their contribution to climate change in the future. Large scale ice sheets behave as incompressible non-Newtonian fluid. The evolution of ice sheet is governed by the conservation laws of mass, momentum and energy, which is formulated as a system of partial differential equations. Improving the efficiency of numerical ice sheet modeling is always a desirable feature since many of the applications have large domain and aim for long time span. With such a goal, the first part of this thesis focuses on developing efficient and accurate numerical methods for ice sheet simulation.

A large variety of physical processes are involved in ice dynamics, which are described by physical laws with parameters measured from experiments and field work. These parameters are considered as the inputs of the ice sheet simulations. In certain circumstances, some parameters are unavailable or can not be measured directly. Therefore, the second part of this thesis is devoted to reveal these physical parameters by solving inverse problems.

In the first part, improvements of temporal and spatial discretization methods and a sub-grid boundary treatment are purposed. We developed an adaptive time stepping method in Paper I to automatically adjust the time steps based on stability and accuracy criteria. We introduced an anisotropic Radial Basis Function method for the spatial discretization of continental scale ice sheet simulations in Paper II. We designed a sub-grid method for solving grounding line migration problem with Stokes equations in Paper VI.

The second part of the thesis consists of analysis and numerical experiments on inverse problems. In Paper IV and V, we conducted sensitivity analysis and numerical examples of the inversion on time dependent ice sheet simulations. In Paper III, we solved an inverse problem for the thermal conductivity of firn pack at Lomonosovfonna, Svalbard, using the subsurface temperature measurements.

Keywords: ice sheet modeling, finite element method, grounding line migration, inverse problems, adjoint method

Gong Cheng, Department of Information Technology, Division of Scientific Computing, Box 337, Uppsala University, SE-751 05 Uppsala, Sweden. Department of Information Technology, Numerical Analysis, Box 337, Uppsala University, SE-75105 Uppsala, Sweden.

© Gong Cheng 2019

ISSN 1651-6214

ISBN 978-91-513-0738-1

urn:nbn:se:uu:diva-392268 (<http://urn.kb.se/resolve?urn=urn:nbn:se:uu:diva-392268>)

Dedicated to my parents

List of papers

This thesis is based on the following papers, which are referred to in the text by their Roman numerals.

- I G. Cheng, P. Lötstedt and L. von Sydow. Accurate and stable time stepping in ice sheet modeling. *Journal of Computational Physics*, Vol. 329, pp. 29–47, 2017.
- II G. Cheng and V. Shcherbakov. Anisotropic radial basis function methods for continental size ice sheet simulations. *Journal of Computational Physics*, Vol. 372, pp. 161–177, 2018.
- III S. Marchenko, G. Cheng, P. Lötstedt, V. Pohjola, R. Pettersson, W. van Pelt and C. Reijmer. Thermal conductivity of firn at Lomonosovfonna, Svalbard, derived from subsurface temperature measurements. *The Cryosphere*. Vol. 13, pp. 1843–1859, 2019
- IV G. Cheng and P. Lötstedt. Parameter sensitivity analysis of dynamic ice sheet models. Available as arXiv: 1906.08197, 2019. (submitted)
- V G. Cheng and P. Lötstedt. Parameter sensitivity analysis of dynamic ice sheet models–numerical computations . *The Cryosphere Discuss.*, <https://doi.org/10.5194/tc-2019-151>, in review, 2019.
- VI G. Cheng, L. von Sydow and P. Lötstedt. A subgrid model for the simulation of grounding line migration in icesheet modeling using Nitsche’s method. Available as arXiv: 1908.10751, 2019. (submitted)

Reprints were made with permission from the publishers.

Related Work

The following paper, although not explicitly discussed in the comprehensive summary, is related to the contents of this thesis.

- [20] E. C. H. van Dongen, N. Kirchner, M. B. van Gijzen, R. S. W. van de Wal, T. Zwinger, G. Cheng, P. Lötstedt and L. von Sydow. Dynamically coupling full Stokes and shallow shelf approximation for marine ice sheet flow using Elmer/Ice (v8.3). *Geoscientific Model Development*, Vol. 11, pp. 4563–4576, 2018.

Contents

1	Introduction	11
2	Ice Sheet Modeling	14
2.1	The Stokes Equations	15
2.2	Approximations of the Stokes Equations	17
2.2.1	Blatter-Pattyn Model	17
2.2.2	SSA	19
2.2.3	SIA	19
2.2.4	Hybrid Models	19
2.3	Time Dependency	20
2.4	Inverse Problems	21
3	Numerical Methods	24
3.1	Spatial Discretization	24
3.1.1	The Finite Element Method	24
3.1.2	Subgrid Treatment for Grounding Line	25
3.1.3	The Radial Basis Function Method	27
3.2	Temporal Discretization	29
4	Summary of Papers	31
4.1	Paper I	31
4.2	Paper II	31
4.3	Paper III	31
4.4	Paper IV	32
4.5	Paper V	32
4.6	Paper VI	32
5	Acknowledgment	34
6	Summary in Swedish	35
	References	36

1. Introduction

Ice sheets are continental size of ice covering large areas of land. Currently, there are two ice sheets existing on the earth, the Antarctica and the Greenland ice sheet. During the past, there were a few more palaeo ice sheets. For instance, at the Last Glacial Maximum when ice sheets reached their maximal extent in the most recent time at about 26,500 years ago, the Laurentide Ice Sheet covered North America and the Scandinavian ice sheet covered most of northern Europe.

The ice sheets have strong impact on the climate system. They are essential to the global warming as the ice and snow on the earth surface reflect solar radiation back into the space. And, the mass loss of ice sheets contributes to the sea level rise [19, 54]. One direct observation of the ice loss in Antarctica is the retreat of the grounding line, which is the transient zone between the grounded and floating ice. Numerical experiments have shown the instability of the grounding line on the bedrock sloping up towards the ocean [89, 104], which is the configuration in the West Antarctic ice sheet [63]. According to the IPCC special report on global warming in 2018, a projection of 1.5°C global warming between 2030 and 2052 is expected comparing to the pre-industrial levels. In this sense, studying the ice dynamics, especially with the help of numerical simulations, is important to understand our world and predict for the future.

The physical process of the ice sheet is governed by the so-called Stokes equations, or full Stokes equations (FS) in some literatures [38]. They consist of the conservation laws of mass, momentums and energy, which are described by a system of partial differential equations (PDEs). Due to the nature of the ice, there is a strong nonlinear effect involved in the ice dynamics which makes the PDEs difficult to be solved. Therefore, a lot of effort has been made by researchers to simplify the ice sheet models for efficiency concerns, such as the Blatter-Pattyn model [7, 72, 102], Shallow Shelf Approximation (SSA) [59, 66], Shallow Ice Approximation (SIA) [45], etc. However, each of these approximations is only appropriate for parts of the ice sheet and they are proved to be inaccurate in other regions, respectively. To improve the accuracy, hybrid models are developed to couple several approximations together or with the Stokes equations. The coupling can be done statically based on the geometry [12, 36, 82] or dynamically according to the numerical solutions [3, 20].

Previous studies suggest that the approximations and hybrid models are accurate enough in many places [46, 75, 77, 96], but it is necessary to use the

Stokes equations to capture all the stress components at the grounding line region [68]. Numerical experiments are conducted to investigate the modeling and numerical properties of the grounding line migration problems, especially the choice of the friction law. For example, the basal shear stress in the Coulomb friction law decreases to zero when approaching the grounding line, whereas it increases in the Weertmann law as the velocity getting larger [104, 108]. Different transient behaviors are observed with the same initial condition but different friction laws [11]. In addition, there is a strong resolution dependency close to the grounding line which may limit the efficiency of the computation [28, 77]. Many attempts have been made to improve the efficiency and accuracy of the solution method, such as to include the effective pressure into the friction laws for a detailed representation of the grounding line [11, 88, 90, 104], a predefined parameterization of the transition zone based on the geometric information of the domain [28, 74], and a subgrid grounding line parameterization with SSA by considering the hydrostatic condition [95]. The results suggest that a detailed subgrid treatment of the physical process at the grounding line can improve the accuracy of the solutions without losing the efficiency of the numerical method.

However, direct observations of the basal conditions are not always accessible or practically impossible to acquire [35]. Inverse problems are constructed and solved for the unobservable parameters in ice sheet modeling [27, 61, 64]. The top surface observations, such as the height and the velocities, can be used to invert for the bottom surface elevation and basal friction coefficients [42]. These inverse problems are proved to be well-posed in the fast flowing region [69]. The most commonly applied inversion technique in ice sheet modeling is the adjoint method [47, 60, 61, 81], which is used in minimizing the mismatch between the targeted variables in the model and the observations. During the solution procedure, the gradient of the mismatch function is computed by the adjoint method, which provides the sensitivity of the targeted variables [31]. Other physical parameters of the ice can be evaluated in a similar way, such as the thermal diffusivities of the snow/firn pack [93], the viscosity of the ice [27], etc. The other inverse methods such as Bayesian approach [42, 84] and inverse Robin method [5] were developed early on, but they are not widely used anymore in ice sheet modeling since the adjoint method is more efficient and robust. Recently, the time dependent inverse problem has started to attract more attention [34] since it provides a possibility to use observations from transient flow and to estimate the initial condition without spin-up simulations [73].

A variety of tools and softwares are developed for solving problems in ice sheet modeling with different numerical methods. The finite difference method is used in the Parallel Ice Sheet Model (PISM) [12, 110] to solve a hybrid SIA-SSA model. Due to the simplification of the model and the efficiency of the finite difference method, PISM is able to run large scale simulations up to 10^5 years [83]. The finite element method is broadly used in many appli-

cations such as the Ice Sheet System Model (ISSM) [55], Elmer/ICE [30], Albany/FELIX [102, 103], etc. These softwares utilize the flexibility of the finite element method and are able to handle problems on realistic geometries. The finite volume method is applied in BISICLES for a vertically integrated ice model [18, 91]. Both the finite element method and finite volume method are combined with adaptive mesh refinement to achieve better performance. The radial basis function (RBF) methods are implemented for modeling ice dynamics, which has the advantage to handle moving boundaries with the meshfree nature [4].

The rest of the thesis is divided into three parts: Chapter 2 covers the mathematical models of the ice dynamics including both the forward models and the inverse problems. Chapter 3 introduces the numerical methods used for solving the ice models. And, the summary of the papers is given in Chapter 4.

2. Ice Sheet Modeling

Ice in large scale, such as ice sheets and glaciers, behaves as a fluid. The deformations and motions are mainly driven by the gravity force [38]. The responses from climate forcing in ice sheet modeling can be included as external forces or boundary conditions, for instance, mass balance, isostatic adjustment of the lithosphere, heat transfer, etc. In addition, the ice-ocean interaction is taken into account as a boundary condition on the ice shelf in marine ice sheet models.

An ice sheet or glacier usually occupies a three dimensional (3D) shallow domain with large aspect ratio (ratio of the width to the height of the domain). Conventionally, the vertical direction is always denoted by z and the horizontal coordinates consist of x and y . A 3D sketch is shown in Figure 2.1 with exaggeration in the z -direction, whereas a slice in the z -direction following a central flow line establishes a two-dimensional (2D) problem.

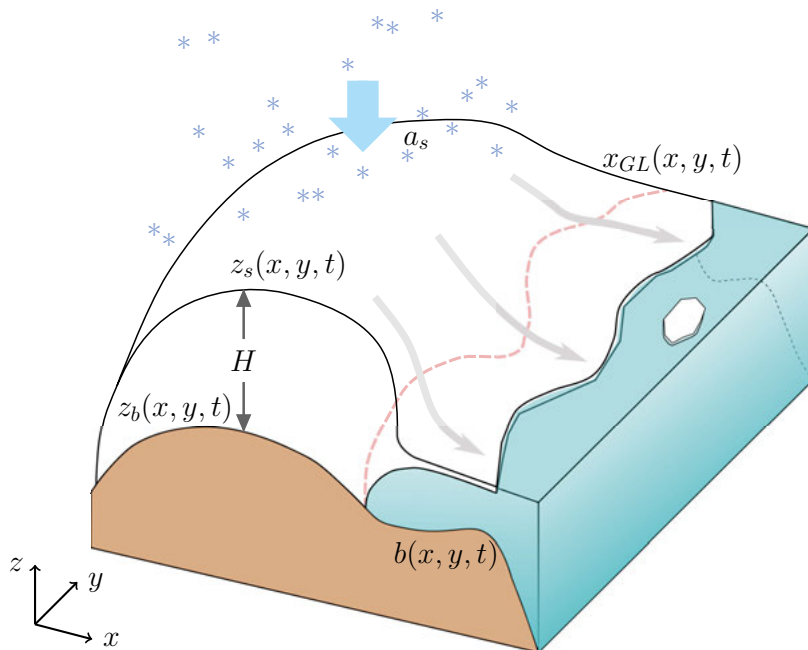


Figure 2.1. A three-dimensional schematic view of an ice sheet. The dashed red line indicates the grounding line.

Denote the whole ice domain by Ω , the top surface by Γ_s and the bottom surface by Γ_b . Due to the shallowness of Ω , the top and bottom surfaces are assumed to be uniquely determined by the x and y coordinates at a given time t . A general notation for the top surface is $z = z_s(x, y, t)$ and the bottom surface is $z = z_b(x, y, t)$. The thickness of the ice is defined as $H = z_s - z_b$, see Figure 2.1.

In marine ice sheets, $z_b(x, y, t)$ coincides with the bedrock $b(x, y, t)$ on the grounded part and $z_b(x, y, t) > b(x, y, t)$ defines the floating part. The transition zone between the grounded and floating ice is called the grounding line. The red dashed line in Figure 2.1 illustrates a grounding line $\mathbf{x}_{GL}(x, y, t)$ on the bottom surface of the ice. In 2D flow-line problems, the grounding line position is reduced to a single point on the ice bottom.

The thick blue arrow on top of the ice sheet in Figure 2.1 demonstrates the surface mass balance function $a_s(x, y, t)$. It can be both positive and negative which refers to accumulation and ablation, respectively. In the interior region of the ice sheet, accumulations are mainly due to the precipitation which directly contributes to the increase of the surface elevation. The mass ablations, mainly melting, can happen both on the top and bottom surfaces by the heat transferring from the air, geothermal heating beneath the grounded ice, as well as the interaction between the floating ice and the sea water.

Let $\mathbf{u} = (u_1, u_2, u_3)^T$ be the velocity field and p be the pressure of the ice with the 3D coordinates $\mathbf{x} = (x, y, z)$. For the rest of the thesis, a variable with numbers in the subscripts refers to the component in different spatial dimensions and the subscript x, y, z or t represents a derivative with respect to the subscript of the variable. A more detailed definition of the domain and the notations is described in Paper IV.

2.1 The Stokes Equations

The dynamics of ice is governed by the Stokes equations

$$\begin{cases} \nabla \cdot \mathbf{u} = 0, \\ -\nabla \sigma = \mathbf{f}, \end{cases} \quad (2.1)$$

where σ is the Cauchy stress tensor and $\mathbf{f} = (0, 0, -\rho g)^T$ is the gravitational force with the ice density ρ and the gravitational acceleration g . The Cauchy stress tensor is defined as $\sigma(\mathbf{u}, p) = 2\eta(\mathbf{u})\mathbf{D}(\mathbf{u}) - \mathbf{I}p$ with the viscosity $\eta(\mathbf{u})$, the strain rate $\mathbf{D}(\mathbf{u}) = \frac{1}{2}(\nabla\mathbf{u} + \nabla\mathbf{u}^T)$ and an identity matrix \mathbf{I} .

The viscosity is governed by the Glen's flow law [33, 38] as

$$\eta(\mathbf{u}) = \frac{1}{2}A(T)^{-\frac{1}{n}}\mathbf{D}_e(\mathbf{u})^{\frac{1-n}{2n}} \quad (2.2)$$

where $A(T)$ is the rate factor depending on the ice temperature T , $\mathbf{D}_e(\mathbf{u}) = \text{tr}\mathbf{D}^2(\mathbf{u})$ is the trace of \mathbf{D}^2 and $n \geq 1$ is called the stress exponent. One typical

choice of the stress exponent for ice is $n = 3$, see in [33, 38, 71]. However, for $n > 1$ in (2.2), the viscosity $\eta(\mathbf{u})$ is singular when $\mathbf{D}_e(\mathbf{u}) = \mathbf{0}$. This may not ruin the wellposedness of (2.1) by letting $\eta(\mathbf{u})\mathbf{D}(\mathbf{u}) = \mathbf{0}$ as $\mathbf{D}(\mathbf{u}) = \mathbf{0}$ [13], but it will cause numerical difficulties for the nonlinear solver to converge [102]. One common remedy is to add a small regularization term in (2.2) such that

$$\eta(\mathbf{u}) = \frac{1}{2}A(T)^{-\frac{1}{n}}(\mathbf{D}_e(\mathbf{u}) + \eta_0)^{\frac{1-n}{2n}}, \quad (2.3)$$

where $0 < \eta_0 \ll 1$. The value of η_0 can be either a small positive constant [38] or updated according to a homotopy continuation algorithm as in [102].

In paleoclimate models, the rate factor is usually related to the climate forcing such that $A(T)$ increases in the warming period and decreases during the cooling period. The temperature of the ice is obtained by solving a time dependent energy balance equation [38] which is derived from the Fourier's law of heat conduction. The model of ice temperature and heat transfer is discussed in Section 2.3.

The boundary conditions on the top, bottom and lateral surfaces of the domain are specified to close the system and to provide a unique solvable problem. On the top surface, as the atmospheric pressure and the wind stress are negligible comparing to the stresses in the ice sheet, a stress free boundary is imposed such that

$$\boldsymbol{\sigma}\mathbf{n} = \mathbf{0}, \quad (2.4)$$

where \mathbf{n} is the outward normal vector on the surface.

The bottom surface consists of several different boundary conditions depending on the types of the interfaces. If the basal temperature of the grounded ice is below the pressure melting point such that the ice is frozen on the bedrock, then a no-slip condition is given as

$$\mathbf{u} = \mathbf{0}. \quad (2.5)$$

Otherwise, a slip condition is imposed. The physical processes beneath the ice is complicated and difficult to be measured directly. It is not entirely clear how to accurately describe the friction law [65, 99]. However, the friction boundary condition appears to be crucial in many applications [11, 32, 49, 104]. Among these, a general relationship between the basal velocity and the basal shear stress can be established that

$$\mathbf{T}\boldsymbol{\sigma}\mathbf{n} = -\beta(\mathbf{u})\mathbf{u}, \quad \mathbf{u} \cdot \mathbf{n} = 0, \quad (2.6)$$

where $\mathbf{T} = \mathbf{I} - \mathbf{n} \otimes \mathbf{n}$ is a projection on the tangential plane with the Kronecker outer product ' \otimes ', see [81] and Paper IV. The friction coefficient $\beta(\mathbf{u}) \geq 0$ can be a linear or nonlinear scalar function of the basal velocity \mathbf{u} based on the choice of the friction law as in [29, 87, 104, 108].

At the ice-ocean interface, the friction is zero, so the boundary condition is given as in [23]

$$\mathbf{T}\boldsymbol{\sigma}\mathbf{n} = \mathbf{0}, \quad \boldsymbol{\sigma}\mathbf{n} = -p_w\mathbf{n}, \quad (2.7)$$

where the outward normal vector \mathbf{n} is pointing from the ice to the sea water and p_w is the water pressure at the depth of the interface.

2.2 Approximations of the Stokes Equations

The Stokes equations (2.1) are difficult to solve because of the highly nonlinear viscosity and the saddle point problem that arises from the discretization [8, 43, 56]. It may not be affordable to simulate 3D Stokes equations for an ice sheet over long time span due to the high computational demand in storage and time [30, 92, 113]. Improving efficiency of the numerical methods for ice sheet modeling attracts much attention [44, 48, 105]. On the other hand, there are many uncertainties in ice dynamics [19, 86] since some physical processes involved are still unclear or difficult to model, such as the initial conditions [73], basal frictions [65, 100], grounding line migration [32], etc. Much effort has been spent on simplifying the models as long as the approximation errors do not overwhelm the uncertainty in the models.

Most of the simplifications [1, 39, 45, 55, 59, 67, 72] are based on the fact that the ice sheet has a low aspect ratio α , which is the ratio between the height and the width of the domain [21, 102]. Since the vertical normal stress (σ_{33} in Figure 2.2) dominates, a hydrostatic approximation [21, 72, 91] is made such that the other shear stresses in the vertical direction (σ_{31} and σ_{32} in Figure 2.2, marked in color green) can be neglected. Then, the momentum balance equation (2.1) in the vertical direction is reduced to

$$\frac{\partial \sigma_{33}}{\partial z} \approx \rho g. \quad (2.8)$$

Integrating (2.8) from the top surface z_s to a depth z gives

$$\sigma_{33}(z) = -\rho g(z_s - z), \quad (2.9)$$

which is another form of the hydrostatic approximation. Combining with the definition of the Cauchy stress tensor, the unknown pressure p in the Stokes equations (2.1) can be expressed by a function of u_3 through this approximation.

2.2.1 Blatter-Pattyn Model

The Blatter-Pattyn model was first established by Blatter [7] in 1995 and simplified by Pattyn [72] in 2003. The major assumption is based on the low aspect ratio of the domain that the horizontal variations of the vertical velocity is negligibly small comparing to the other components in the shear stresses σ_{13} and σ_{23} . Using the hydrostatic approximation in (2.8), the Stokes equations

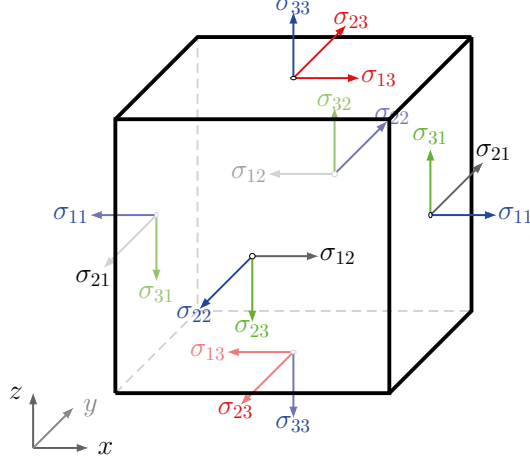


Figure 2.2. A schematic view of the stress components. The normal stresses are in blue and the shear stresses on the horizontal planes are in red. The shear stresses in the vertical direction are in green.

(2.1) are approximated by the Blatter-Pattyn model with only two unknowns u_1 and u_2 to satisfy

$$\nabla \cdot \boldsymbol{\sigma}_{BP}(u_1, u_2) = \rho g \nabla z_s, \quad (2.10)$$

where $z_s(x, y)$ is the surface elevation and the stress tensor of the Blatter-Pattyn model is defined as

$$\boldsymbol{\sigma}_{BP}(u_1, u_2) = \eta_{BP}(u_1, u_2) \begin{bmatrix} 4 \frac{\partial u_1}{\partial x} + 2 \frac{\partial u_2}{\partial y} & \frac{\partial u_1}{\partial y} + \frac{\partial u_2}{\partial x} & \frac{\partial u_1}{\partial z} \\ \frac{\partial u_1}{\partial y} + \frac{\partial u_2}{\partial x} & 2 \frac{\partial u_1}{\partial x} + 4 \frac{\partial u_2}{\partial y} & \frac{\partial u_2}{\partial z} \\ \frac{\partial u_1}{\partial z} & \frac{\partial u_2}{\partial z} & 0 \end{bmatrix}, \quad (2.11)$$

with the viscosity $\eta_{BP}(u_1, u_2)$ which is approximated by neglecting $\frac{\partial u_3}{\partial x}$ and $\frac{\partial u_3}{\partial y}$ and replacing $\frac{\partial u_3}{\partial z} = -(\frac{\partial u_1}{\partial x} + \frac{\partial u_2}{\partial y})$ in (2.2) or (2.3). The detailed formula of $\eta_{BP}(u_1, u_2)$ is given in Paper II.

The boundary conditions for the Blatter-Pattyn model are the same as in (2.4)-(2.7) for the Stokes equations, except that the stress tensor is $\boldsymbol{\sigma}_{BP}$ as in (2.11).

After solving (2.10) with appropriate boundary conditions for (u_1, u_2) , the vertical velocity u_3 and the pressure p are recovered through the mass balance equation $\nabla \cdot \mathbf{u} = 0$ and the hydrostatic approximation (2.8), respectively. If (2.1) considers a 2D problem, then the corresponding Blatter-Pattyn approximation will only have u_1 as the unknown. The reduction of the unknowns makes the Blatter-Pattyn model easier to be parallelized and solved comparing to the Stokes equations [103].

The Blatter-Pattyn model is also called the first-order approximation of the Stokes equations as it is in the order of $\mathcal{O}(\alpha)$ accurate [7, 72, 91, 102]. Numer-

ical experiments have shown that the solution of the Blatter-Pattyn model is in good agreement with those from the Stokes equations as long as the domain has a low aspect ratio with small basal slope [44, 72, 75, 79].

2.2.2 SSA

The SSA assumes a plug flow on the ice shelf and in the fast flowing area [38], where horizontal velocities are constant in the vertical direction. This leads to a further simplification from the hydrostatic approximation that all the vertical variations are neglected [59, 89].

As a result, a 3D ice problem is reduced by the SSA to a 2D problem in the x - y plane with the unknowns $\mathbf{u} = (u_1, u_2)$ and the boundary conditions become one dimensional on the outline of the domain. The governing equations of the SSA are derived by vertically integrating the momentum balance equations from the basal friction condition to the top free surface [38]. The details of the SSA equations are given in Paper IV. This approximation is widely used for grounding line migration problems both in analysis and numerical experiments [77, 90].

2.2.3 SIA

Unlike the ice shelf, the inland ice sheet exhibits a completely different behavior where the bed parallel shear stresses dominate [38, 45], seen as σ_{13} and σ_{23} in Figure 2.2 in color red. These two stresses are further approximated by $\sigma_{13} \approx \eta(\mathbf{u}) \frac{\partial u_1}{\partial z}$ and $\sigma_{23} \approx \eta(\mathbf{u}) \frac{\partial u_2}{\partial z}$ due to the low aspect ratio of the domain. By assuming that all normal stresses are equal to the pressure, the shallow ice approximation is achieved [1, 2, 67] where the horizontal velocity is explicitly expressed by an integral expression in the vertical direction, see in Paper I.

The SIA is shown to be accurate in low aspect ratio domain both analytically and numerically [3, 46, 78, 91], except for the areas where the assumptions are no longer valid, such as on the ice shelf, close to the grounding line and on the ice dome region. The approximation is very cheap to compute, especially useful in palaeo ice sheet simulations [52].

2.2.4 Hybrid Models

All the approximations mentioned in Sections 2.2.1–2.2.3 are simplifications of the Stokes equations based on some prior knowledge of the target area. These models can be used to replace the Stokes equations with less computational demand at the specific regions on the ice sheet and shelf where the assumptions are valid, but may be inadequate for the other parts of the ice. Since each of these approximations can not cover the whole ice sheet, one

common idea is to simulate the continental-size ice sheet with different models for different regions and couple them dynamically [3, 20, 96].

The Parallel Ice Sheet Model (PISM) [12, 82, 110] uses the SSA solution as the sliding velocity in the SIA model and combines them with a weight function which depends on the magnitude of the SSA velocity. The SIA-SSA coupling only requires the solution of a PDE on the horizontal plane for the SSA velocities which makes it accessible for simulation of large scale ice sheets over long time spans.

However, at some particular areas, e.g., at the domes, ice margin and grounding line, the Stokes equations are necessary [28, 76, 77]. Therefore, approximations coupled with the Stokes equations are developed. The Ice Sheet Coupled Approximation Levels (ISCAL) method [3] automatically determines the domain of Stokes equations and SIA by dynamically estimating the modeling error. It can be up to nine times faster than using the Stokes equations everywhere with less than 5% relative error. Examples are shown in [3, 52] and Paper I.

Another approach to couple SSA with the Stokes equations is developed in [20] where the SSA domain is determined dynamically on the ice shelf with a certain distance from the grounding line. Special boundary conditions are imposed at the coupling interface since there is a mismatch of the dimensions in this hybrid model as SSA is only defined on the horizontal plane. The reduction of dimensions in SSA reduces the computational complexity and memory usage when solving problems with large ice shelves.

These hybrid models make it possible to efficiently reconstruct the 3D palaeo ice sheet with high resolution [52, 83, 101] and to predict sea level rise in the near future with decent accuracy [6, 37].

2.3 Time Dependency

Temporal variations are introduced to ice models by the moving surfaces, see [30, 38] and Paper I. Consider the top surface $z_s(x, y, t)$ and the bottom surface $z_b(x, y, t)$, the evolution of the two surfaces are governed by

$$\frac{\partial z_c}{\partial t} + u_1 \frac{\partial z_c}{\partial x} + u_2 \frac{\partial z_c}{\partial y} = a_c + u_3, \quad (2.12)$$

where $c = s$ or b . The mass balance function is referred as a_c where $a_s \geq 0$ represents the surface accumulation rate and $a_b \geq 0$ is the basal melting rate. These two surface functions are only defined on the $x - y$ plane and the velocity components used in the equations are obtained on the top and bottom boundaries of the domain Ω . In this sense, (2.12) is called the kinematic boundary condition [38].

Another way to express the motion of the ice is through the thickness H as

$$\frac{\partial H}{\partial t} + \frac{\partial q_1}{\partial x} + \frac{\partial q_2}{\partial y} = a_s - a_b, \quad (2.13)$$

where $q_1 = \int_{z_b}^{z_s} u_1 dz$ and $q_2 = \int_{z_b}^{z_s} u_2 dz$ are the volume fluxes. Actually, (2.13) is derived by integrating the mass conservation equation $\nabla \cdot \mathbf{u} = 0$ vertically and replacing some terms by z_b and z_s in (2.12) [38]. Knowing two variables among z_s , z_b and H , the geometry of the ice at any given time t can be uniquely determined. In some cases, z_b is fixed in time, then (2.12) for z_s or (2.13) is used as an alternative to each other, seen as in Paper I.

Another time dependent variable of the ice is the temperature T which is governed by the Fourier's law of heat conduction as

$$\rho C \left(\frac{\partial T}{\partial t} + \mathbf{u} \cdot \nabla T \right) = \nabla \cdot (k \nabla T) + \zeta, \quad \mathbf{x} \in \Omega, \quad (2.14)$$

where $C(\mathbf{x})$ is the specific heat capacity, $k(\mathbf{x})$ is the effective thermal conductivity and $\zeta(\mathbf{u})$ is the internal energy due to viscous deformation [30, 55]. In the firm model, velocity variations are small so that the terms with \mathbf{u} in (2.14) are neglected, seen as Paper III.

The coupling of the time dependent equations to the Stokes equations or the other approximations leads to a system of differential algebraic equations (DAEs) [53], which may restrict the choice of the time stepping method, see Paper I. This content is discussed in Section 3.2.

2.4 Inverse Problems

Physical parameters are essential to ice modeling, but some of them are difficult to be measured or obtained directly, for instance, the thermal conductivity [85], the basal friction conditions [61, 106], the viscosity and flow law coefficients [107], etc. The inverse method plays an important role in retrieving these parameters from observations by constructing a minimization problem in which the objective function is the mismatch between the model variables and the measured data [21, 30, 61, 81].

Denote a general form of the forward problem as

$$F(v(\xi), q(\xi)) = R(q(\xi)), \quad \xi \in \Psi, \quad (2.15)$$

where Ψ is the computational domain including space and time, ξ are the variables on Ψ . If the forward problem is time dependent, then $\xi = (\mathbf{x}, t)$, otherwise, $\xi = \mathbf{x}$. The governing equations are represented by F with the right-hand-side R , $v(\xi)$ are the unknown variables and $q(\xi)$ are the parameters. The initial and boundary conditions are given as

$$B(v(\xi), q(\xi)) = G(q(\xi)), \quad \xi \in \partial\Psi. \quad (2.16)$$

The variable v can be the temperature T as in Paper III or the flow velocities \mathbf{u} as in Paper IV and V. Correspondingly, the parameters q represent the thermal conductivity k , density ρ or the basal friction coefficients β . Other examples of the forward problems are found in [41, 97].

The optimization problem to find the best parameter q is formulated in the least-squares form as

$$q = \arg \min_q \mathcal{J}(v, q) = \arg \min_q \int_{\Psi} J(v, q) d\xi = \arg \min_q \int_{\Psi} w(\xi) (v(q) - \mathcal{V})^2 d\xi, \quad (2.17)$$

where $\mathcal{V}(\xi)$ represents the function of the measurements with a weight function $w(\xi) \geq 0$ and $v(q)$ is the solution of the forward problem with the given q . The weight function $w(\xi)$ is nonzero when there is measured data at ξ and the function $\mathcal{V}(\xi) = 0$ as long as $w(\xi) = 0$. The procedure to solve for (2.17) with the forward equations in (2.15) and (2.16) as constraints is called the inverse problem.

Actually, the minimization problem in (2.17) is equivalent to find q such that

$$\frac{\partial \mathcal{J}(v(q), q)}{\partial q} = \frac{\partial \mathcal{J}}{\partial q} + \frac{\partial \mathcal{J}}{\partial v} \frac{\partial v}{\partial q} = 0. \quad (2.18)$$

If $v(q)$ is given explicitly as a function of q or the dimensions of q is small, then the inverse problem can be solved directly by computing the derivatives $\frac{\partial v}{\partial q}$ in (2.18) from the analytical expression of $v(q)$ or numerically [41].

However, in ice sheet modeling, v is usually the velocity or surface elevation which are governed by a system of PDEs and the targeted physical parameters q vary in space and time. Then the direct method to calculate $\frac{\partial v}{\partial q}$ may be impractical. In this case, the adjoint method is introduced by constructing the Lagrangian function of the optimization problem as

$$\mathcal{L}(q, \varphi) = \mathcal{J}(v, q) + \int_{\Psi} (F(v, q) - R(q)) \varphi d\xi + \int_{\partial\Psi} (B(v, q) - G(q)) \varphi d\xi, \quad (2.19)$$

where $\varphi(\xi)$ is the so-called Lagrange multiplier and the solution to (2.18) also minimizes (2.19) for any value of φ with the forward problem satisfied.

Take the q -derivative of the Lagrangian \mathcal{L} and rearrange the terms as

$$\begin{aligned} \frac{\partial \mathcal{L}}{\partial q} = & \frac{\partial \mathcal{J}}{\partial q} + \int_{\Psi} \left(\frac{\partial J}{\partial v} + \frac{\partial F}{\partial v} \varphi \right) \frac{\partial v}{\partial q} d\xi + \int_{\partial\Psi} \frac{\partial B}{\partial v} \frac{\partial v}{\partial q} \varphi d\xi \\ & + \int_{\Psi} \left(\frac{\partial F}{\partial q} - \frac{\partial R}{\partial q} \right) \varphi d\xi + \int_{\partial\Psi} \left(\frac{\partial B}{\partial q} - \frac{\partial G}{\partial q} \right) \varphi d\xi. \end{aligned} \quad (2.20)$$

To eliminate all the terms with $\frac{\partial v}{\partial q}$, the Lagrange multiplier φ is chosen such that

$$\begin{aligned}\frac{\partial F}{\partial v}\varphi + \frac{\partial J}{\partial v} &= 0, \quad \xi \in \Psi, \\ \frac{\partial B}{\partial v}\varphi &= 0, \quad \xi \in \partial\Psi.\end{aligned}\tag{2.21}$$

The procedure of calculating the q -derivative of \mathcal{L} with a given q_0 is as following. Firstly, the forward problem (2.15) is solved with (2.16) at the given q_0 to get v_0 . Then, the adjoint variable φ_0 is solved from (2.21) using the forward solution v_0 . Finally, the adjoint solution φ_0 is inserted into the derivative equation (2.20) together with q_0 to get $\frac{\partial \mathcal{L}}{\partial q}$. Therefore, the optimal q of the minimization problem in (2.17) is found by a gradient-based method which calculates $\frac{\partial \mathcal{L}}{\partial q}$ during every nonlinear iteration.

Furthermore, the forward problem F in (2.15) may contain some spatial or temporal derivatives of v , then there will be additional terms in the partial derivatives in (2.20). These terms can be added to the adjoint equation by transforming the derivatives to have the common multiplier $\frac{\partial v}{\partial q}$ using integration by parts. More detailed examples are shown in the appendix of Paper IV and in [97]. The adjoint methods are widely used to solve inverse problems on ice sheet modeling for the Stokes equations [81], SSA [61] and the Blatter-Pattyn model [21, 35]. Due to the nonlinearity of the ice viscosity, there are incomplete and complete adjoints corresponding to forward problems. These adjoints are compared in [35] within a hybrid model and in Paper V for SSA. In general, there are no major differences between the two adjoint solutions, but the complete adjoint is more accurate. For time dependent problem, since error accumulates, the complete adjoint is preferable.

Another application of the adjoint methods in ice sheet modeling is to investigate the parameter sensitivity and uncertainty [42, 47, 80]. Instead of solving for a minimization problem as in (2.17) with a least-square form objective function, only the derivative of the Lagrangian in (2.20) is investigated with respect to some other objective functions $J(v, q)$. For instance, $J(v, q) = v(\xi)\delta(\xi - \xi_0)$ defines a point-wise observation on the solution v with the Dirac delta function δ at the given position ξ_0 . Notice that ξ is not restricted to spatial dimensions, time variable is also included. There are more sensitivity analysis and numerical examples shown in Paper IV and V.

3. Numerical Methods

3.1 Spatial Discretization

The computational domain of an ice sheet is usually very shallow with irregular lateral frontiers which can expand or shrink according to the ice dynamics. For simplification, the lateral boundaries are assumed to be parallel to the z -axis so that the domain is determined by the top and bottom surfaces of the ice.

Consequently, discretization methods for complex geometries with unstructured meshes are preferable in solving ice problems, for instance, the radial basis function method [4, 50] in Paper II and the finite element method [10, 30, 55, 102] in Paper I, IV, V and VI. On the other hand, approximation models which can reduce the domain to a simple geometry, such as SSA for 2D problems, tend to use the finite difference method as in [110], Paper IV and V, to simplify the implementations and computations.

3.1.1 The Finite Element Method

One of the commonly used meshes in ice sheet modeling with the finite element method is the vertically extruded mesh [105]. In a 3D problem, it is constructed by first making a structured or unstructured 2D mesh on the x - y plane according to the footprint of the top or bottom surface and then extruding the 2D mesh with the same number of vertical layers which generates prismatic or quadrilateral elements [30]. In this case, the remeshing for the transient problem is trivial since it only requires to move the nodes vertically and the degrees of freedoms remain unchanged. However, the extrusion on the low aspect ratio domain may create highly anisotropic elements which requires special treatments and stabilizations [25, 43, 56].

The mixed weak form of the Stokes equations in (2.1) with the boundary conditions (2.4), (2.6) and (2.7) follows the derivations in [30, 43, 62] as:

Find $(\mathbf{u}, p) \in \mathbf{V}_{k,0} \times M_{k^*}$ such that

$$A((\mathbf{u}, p), (\mathbf{v}, q)) + B(\mathbf{u}, \mathbf{v}) = F(\mathbf{v}), \quad \forall (\mathbf{v}, q) \in \mathbf{V}_{k,0} \times M_{k^*} \quad (3.1)$$

with

$$\begin{aligned}
A((\mathbf{u}, p), (\mathbf{v}, q)) &= \int_{\Omega} 2\eta(\mathbf{u})\mathbf{D}(\mathbf{u}) : \mathbf{D}(\mathbf{v}) - b(\mathbf{u}, q) - b(\mathbf{v}, p), \\
b(\mathbf{u}, q) &= \int_{\Omega} q\nabla \cdot \mathbf{u} \, dx, \\
B(\mathbf{u}, \mathbf{v}) &= \int_{\Gamma_{bg}} \beta \mathbf{u} \cdot \mathbf{v} \, dx \\
F(\mathbf{v}) &= \int_{\Omega} \mathbf{f} \cdot \mathbf{v} \, dx - \int_{\Gamma_{bf}} p_w \mathbf{n} \cdot \mathbf{v} \, dx,
\end{aligned} \tag{3.2}$$

where Γ_{bg} stands for the grounded bottom boundary, Γ_{bf} is the floating bottom boundary and the functional spaces are defined as

$$\mathbf{V}_{k,0} = \left\{ \mathbf{v} \in \left[W^{1,k}(\Omega) \right]^d : \mathbf{v} \cdot \mathbf{n}|_{\Gamma_{bg}} = 0 \right\}, \quad M_{k^*} = \left\{ q : q \in L^{k^*}(\Omega) \right\} \tag{3.3}$$

with $k = 1 + 1/n$, $k^* = 1 + n$ and the spatial dimensions $d = 1, 2$ or 3 .

The weak form in (3.1) leads to a so-called saddle-point problem. In order to have a unique solution, the discretization method has to satisfy the Inf-Sup condition [8, 9, 43, 56]. There are several suitable finite elements for this particular problem, for example, linear Lagrange elements with stabilizations [30, 43], the Taylor-Hood elements [57], an arbitrarily high-order element pairing of $\mathbb{Q}_m \times \mathbb{P}_{m-1}$ with $m > 1$ [48], etc.

The Dirichlet boundary condition $\mathbf{u} \cdot \mathbf{n} = 0$ in (2.6) is strongly imposed in the functional space $\mathbf{V}_{k,0}$. A similar formulation can be used for the no-slip boundary (2.5) as well. The slip boundary (2.6) and the floating ice boundary (2.7) are imposed by replacing the normal or tangential components of the stress tensor in the boundary terms getting from integration by parts [22, 26], some of the derivations are given in Paper VI.

3.1.2 Subgrid Treatment for Grounding Line

Many previous research projects have shown that the grounding line migration problem exhibits modeling and numerical difficulties in determining the exact grounding line positions which is crucial to ice sheet modeling [28, 32, 76, 77, 89]. The dynamics of the ice sheet is sensitive to the treatment close to the grounding line, e.g., the choice of the friction laws [11, 32, 104], parameterization of basal conditions [28, 94, 112], etc.

The grounding line is located at the transition zone between the grounded and the floating ice which separates the slip boundary (2.6) and the floating ice boundary (2.7). There are discontinuities in both the normal and the tangential components of these boundary conditions. In the normal direction, a no-penetration Dirichlet boundary condition $\mathbf{u} \cdot \mathbf{n} = 0$ is prescribed on the grounded side whereas a Neumann type boundary condition $\boldsymbol{\sigma} \mathbf{n} = -p_w \mathbf{n}$ is

imposed by the water pressure on the floating ice. In the tangential direction, the friction coefficient $\beta(\mathbf{u})$ switches from nonnegative to zero at the grounding line. Depending on the choice of the friction law, it is not guaranteed that the friction coefficient is continuous at the grounding line [32].

The discontinuities at the grounding line cause severe mesh resolution dependency in many models including the Stokes equations, the Blatter-Pattyn model, and the SSA, etc. Take the Stokes equations on an ice sheet (typical width is larger than 1000 km) as an example, the mesh size has to be smaller than 200 m close to the grounding line in order to get accurate solutions [23, 28]. This criteria is around 0.5 km in the Blatter-Pattyn model [17] and the SSA [77] for the similar problem size. Moreover, as discussed in Section 2.3 and Paper I, small spatial resolution restricts the time steps. A 200 m mesh size in the Stokes model requires a time step below 0.1 year, which makes it extremely expensive to simulate an ice sheet for 100,000 years.

To improve the efficiency, special numerical treatments are introduced, especially for the palaeo ice sheet simulations. The basic idea is to construct a subgrid model which is able to keep track of the grounding line position within one element and impose different boundary conditions in each part of the element accordingly. This approach has been developed for the SSA with up to 2 km mesh resolutions using finite element method [95] and the Blatter-Pattyn model with 1 km cell size using finite volume method [17].

However, to our knowledge, Paper VI is the first subgrid model of the Stokes equations for grounding line migration problems [94, 111]. The major difficulty in the Stokes equations is how to determine the exact grounding line position. In the SSA or Blatter-Pattyn model, the grounding line position is calculated directly by comparing the hydrostatic and cryostatic pressures as functions of the ice thickness, whereas in the Stokes equations the hydrostatic assumption is not always fulfilled and the pressure p of the ice is involved in the solution [90]. An approximation method is proposed in Paper VI by comparing the normal stress at the ice base and the water pressure on the bedrock in the finite element spaces. This comparison is done in each nonlinear iteration such that the final solution has an estimated grounding line position where the normal stress is balanced by the water pressure. In general, the estimated grounding line position does not necessarily coincide with any nodes.

Then, the friction boundary conditions are imposed by using a high-order integration scheme inside the element with the domain Γ_{bg} and Γ_{bf} separated according to the estimated grounding line position as in [95]. In order to include the no-penetration condition with the dynamically estimated grounding line, the Dirichlet boundary condition is weakly imposed by Nitsche's method as:

Find $(\mathbf{u}, p) \in \mathbf{V}_k \times M_{k^*}$ such that

$$A((\mathbf{u}, p), (\mathbf{v}, q)) + B_\Gamma(\mathbf{u}, p, \mathbf{v}) + B_{\mathcal{N}}(\mathbf{u}, \mathbf{v}, q) = F(\mathbf{v}), \quad \forall (\mathbf{v}, q) \in \mathbf{V}_k \times M_{k^*} \quad (3.4)$$

where $\mathbf{V}_k = \left\{ \mathbf{v} \in [W^{1,k}(\Omega)]^d \right\}$ defines a similar space as $\mathbf{V}_{k,0}$ but without any Dirichlet boundary conditions, A and F are defined as in (3.2), and the boundary term B_Γ is from integration by parts as

$$B_\Gamma(\mathbf{u}, p, \mathbf{v}) = \int_{\Gamma_{bg}} \beta \mathbf{u} \cdot \mathbf{v} \, dx - \int_{\Gamma_{bg}} (\mathbf{n} \cdot \boldsymbol{\sigma}(\mathbf{u}, p) \mathbf{n}) \mathbf{n} \cdot \mathbf{v} \, dx, \quad (3.5)$$

and $B_{\mathcal{N}}$ is based on the Nitsche's method [70] that

$$B_{\mathcal{N}}(\mathbf{u}, \mathbf{v}, q) = \gamma_0 \int_{\Gamma_{bg}} \frac{1}{h} (\mathbf{n} \cdot \mathbf{u})(\mathbf{n} \cdot \mathbf{v}) \, dx - \int_{\Gamma_{bg}} (\mathbf{n} \cdot \boldsymbol{\sigma}(\mathbf{v}, q) \mathbf{n}) \mathbf{n} \cdot \mathbf{u} \, dx, \quad (3.6)$$

with the mesh size h and a constant γ_0 .

Similar contact problem for elastic body has been studied in [15, 16] with a Nitsche-based method, where nonlinear Heaviside functions are formulated to switch between the two types of boundary conditions and the well-posedness is proved in this case.

3.1.3 The Radial Basis Function Method

The radial basis function (RBF) approximation [24] of an arbitrary scalar function $u(\mathbf{x})$ with N scattered nodes $\underline{\mathbf{x}} = [\mathbf{x}_1, \mathbf{x}_2, \dots, \mathbf{x}_N]^T$, $\mathbf{x}_i \in \Omega$ is defined as

$$u(\mathbf{x}) \approx \tilde{u}(\mathbf{x}) = \sum_{j=1}^N \lambda_j \phi(\varepsilon, \|\mathbf{x} - \mathbf{x}_j\|), \quad \mathbf{x} \in \Omega, \quad (3.7)$$

where λ_j are the unknown coefficients and $\phi(\varepsilon, \|\mathbf{x} - \mathbf{x}_j\|)$ is a radial basis function centered at \mathbf{x}_j with shape parameter ε . Typical choices of the radial basis functions are shown in Table 2 of Paper II. With a given shape parameter ε , the value of the basis function ϕ only depends on the distance from a node \mathbf{x} to the center of the basis function \mathbf{x}_j . In this case, the distance is defined by the Euclidean norm. The shape parameter ε determines the width of the radial basis function which is usually chosen empirically [4].

The coefficients $\underline{\lambda} = [\lambda_1, \lambda_2, \dots, \lambda_N]^T$ are computed by collocating (3.7) at the node set $\underline{\mathbf{x}}$ with the interpolation condition and solving the linear system

$$A \underline{\lambda} = \underline{u} \quad (3.8)$$

where $\underline{u} = [u(\mathbf{x}_1), u(\mathbf{x}_2), \dots, u(\mathbf{x}_N)]^T$ and A is an $N \times N$ matrix with $A_{ij} = \phi(\|\mathbf{x}_i - \mathbf{x}_j\|)$, $i, j = 1, 2, \dots, N$.

The RBF method is used to solve PDEs [50, 51] by applying the differential operators on the RBF approximations and collocating at the scattered points $\underline{\mathbf{x}}$. Consider a linear PDE on the domain Ω as

$$\mathcal{L}u(\mathbf{x}) = f(\mathbf{x}), \quad (3.9)$$

where \mathcal{L} is the differential operator, u is the solution and f is the right hand side. Substitute $u(\mathbf{x})$ by (3.7) and evaluate the equations at $\underline{\mathbf{x}}$, then

$$L\underline{\lambda} = \underline{f}, \quad (3.10)$$

where $L_{ij} = \mathcal{L}\phi(\|\mathbf{x}_i - \mathbf{x}_j\|)$ and $\underline{f} = [f(\mathbf{x}_1), f(\mathbf{x}_2), \dots, f(\mathbf{x}_N)]^T$. The solution to the PDE (3.9) is recovered by replacing the coefficient $\underline{\lambda}$ with (3.8) such that

$$LA^{-1}\underline{u} = \underline{f}. \quad (3.11)$$

For a smooth radial basis function, LA^{-1} is a dense matrix and (3.11) is called the global RBF method which has exponential convergence for smooth problems [14, 50]. However, as the matrix of the global RBF method is dense, it is expensive to solve (3.11), especially for a large number N . One remedy is to use the RBF partition of unity method (RBF-PUM) which sparsifies the matrix by localizing the radial basis functions.

Define a set of overlapping patches $\{\Omega_k\}_{k=1}^M$ such that

$$\Omega \subset \bigcup_{k=1}^M \Omega_k, \quad (3.12)$$

with the local RBF interpolations on each of the patches as

$$\tilde{u}_k(\mathbf{x}) = \sum_{j=1}^{N_k} \lambda_j^k \phi(\varepsilon, \|\mathbf{x} - \mathbf{x}_j^k\|), \quad \mathbf{x} \in \Omega_k \quad (3.13)$$

where \mathbf{x}_j^k are the nodes covered by the patch Ω_k and N_k is the number of nodes in Ω_k . A patch is usually in circular or spherical shape which can be uniquely determined by the center and the radius.

The RBF-PUM approximation is constructed by summing up all the local approximations from each patch by

$$\tilde{u}(\mathbf{x}) = \sum_{k=1}^M w_k(\mathbf{x}) \tilde{u}_k(\mathbf{x}), \quad (3.14)$$

with the weight functions $\{w_k(\mathbf{x})\}_{k=1}^M$ satisfying

$$\sum_{k=1}^M w_k(\mathbf{x}) = 1, \quad \mathbf{x} \in \Omega. \quad (3.15)$$

Examples of the patches and the weight functions are shown in [4, 109] and Paper II.

Instead of the commonly used Euclidean norm, an anisotropic norm $\|\cdot\|_{\mathbf{a}}$ is defined for the RBF methods to adapt the low aspect ratio in ice sheet modeling. Let \mathbf{r} and \mathbf{s} be two points on Ω , the \mathbf{a} -norm is defined as

$$\|\mathbf{r} - \mathbf{s}\|_{\mathbf{a}}^2 = \sum_{i=1}^d \mathbf{a}_i^2 (\mathbf{r}_i - \mathbf{s}_i)^2, \quad \mathbf{r}, \mathbf{s} \in \Omega \subset \mathbb{R}^d, \quad (3.16)$$

where $d = 2, 3$ is the dimension of the domain and \mathbf{a} is a vector containing the aspect ratio factors with $\mathbf{a}_d = 1$ and $\mathbf{a}_i \ll 1$ for $i = 1, \dots, d - 1$. An example of a 2D anisotropic Gaussian RBF is shown in Figure 2 of Paper II. The patches in RBF-PUM for anisotropic RBFs are also defined as a disc in \mathbf{a} -norm, e.g., Figure 3 of Paper II.

Furthermore, nonlinear problems can be solved in the same manner by first linearizing the equations and then iterating with RBF methods for each linear system. All the differential and interpolation operators can be constructed by the RBF methods before the first nonlinear iteration and applied to the variables during the whole computation. Comparing to the finite element method, the assembling during each nonlinear iteration is replaced by matrix-vector multiplications using RBF matrices. Therefore, a better computational performance is expected by the RBF methods on nonlinear PDEs, especially for large scale and highly parallelizable problems, as suggested in [4] and Paper II.

3.2 Temporal Discretization

The time dependent equations in Section 2.3 are discretized with implicit methods in time for stability reasons [53]. One of the main concerns is the differential algebraic equations [40] resulting from the coupled system.

The general form of a transient ice sheet model is

$$\frac{\partial z_c}{\partial t} + g_1(z_c, \mathbf{u}) = 0, \quad (3.17a)$$

$$g_2(z_c, \mathbf{u}) = 0, \quad (3.17b)$$

where (3.17a) represents the time dependent equations as in Section 2.3 and (3.17b) refers to the Stokes equations or the approximations together with some boundary conditions.

Most of the commonly used solvers are designed for (3.17a) and (3.17b) separately [30, 48, 55, 102, 110] such that it is flexible to use different ice models under the same framework. Denote (z_c^n, \mathbf{u}^n) as the numerical solution at time t^n with the time step $\Delta t_n = t^{n+1} - t^n, n \geq 0$. The solution procedure of the problem in (3.17) at t^n follows:

1. For a given geometry, solve \mathbf{u}^{n+1} from (3.17b) using z_c^n .
2. Advance to z_c^{n+1} by solving time dependent (3.17a) with \mathbf{u}^{n+1} .
3. Update the geometry and states by z_c^{n+1} .

Only one iteration from step 1 to 3 is done at each time step to maintain the efficiency.

However, even with an implicit time stepping method, step 2 in this algorithm is not fully implicit in time since \mathbf{u}^{n+1} is based on the solution z_c^n from the previous time step. Therefore, the stability has to be taken into account when setting the time step. Take (2.12) as an example, the stability of the time

scheme depends on the velocity solution \mathbf{u} and the surface elevation z_c . The detailed analysis is given in Paper I.

In long time simulations, the time step restrictions may vary in a large range which is determined by the combination of the stability and accuracy requirements. Instead of a constant time stepping method, variable step sizes can gain in efficiency without losing accuracy. Paper I presents a predictor-corrector scheme for an adaptive time stepping method [58, 98]. The algorithm for the problem in (3.17) at t^n is:

1. (*Predictor*) Advance to \tilde{z}_c^{n+1} in (3.17a) by an explicit scheme using \mathbf{u}^n .
2. Solve \mathbf{u}^{n+1} in (3.17b) using the predictor \tilde{z}_c^{n+1} .
3. (*Corrector*) Correct the solution of (3.17a) to z_c^{n+1} by an implicit scheme using \mathbf{u}^{n+1} .
4. Estimate the local truncation error τ^{n+1} by comparing the predictor \tilde{z}_c^{n+1} with the corrector z_c^{n+1} .
5. Adjust next time step Δt^{n+1} according to Δt^n , τ^{n+1} , τ^n , etc.

4. Summary of Papers

4.1 Paper I

An adaptive time step control method is introduced for ice sheet simulations based on a predictor-corrector scheme. The discretization errors are estimated by comparing the solutions from two different time stepping methods at each time step, whereas the most expensive procedure, the velocity equation, is solved only once each time step. With a PI-control method applied to the estimated errors, the stability and accuracy of the numerical solutions are maintained. Numerical experiments in 2D and 3D are presented with first and second order time stepping methods. The results are in good agreement with the analysis.

Contribution: The author of this thesis performed the numerical experiments, derived parts of the theory and wrote parts of the manuscript.

4.2 Paper II

This paper introduces an RBF method to simulate continental scale of ice sheets with anisotropic basis functions. An RBF-PUM is also implemented with elliptic patches which has the same aspect ratio as the basis functions. The Blatter-Pattyn model is solved on the ISMIP-HOM B benchmark case and an ice cap geometry. The accuracy and efficiency of the RBF method and RBF-PUM are compared with standard finite element method. The results indicate that the anisotropic RBF-PUM is more efficient and accurate than the other methods in these cases.

Contribution: The paper was made in close collaboration between the two authors.

4.3 Paper III

This paper presents a case study on the thermal conductivity of the firn at Lomonosovfonna, Svalbard, using temperature measurements from 2012 to 2015. A least-squares optimization problem is constructed for the inversion of the effective thermal conductivity and density of the firn with a one-dimensional

heat equations as the constraint. The uncertainties in the targeted parameters are estimated by frequentist techniques. The optimal solution indicates a faster heat conduction of the firn than those found in previous research.

Contribution: The author of this thesis developed the numerical methods and performed the numerical experiments. The manuscript was written by all authors.

4.4 Paper IV

The sensitivity of the top surface observations to the parameters on the bottom surface of the ice sheet is analyzed for time dependent problems. The Stokes equations, SIA and SSA are coupled with the kinematic boundary conditions to create the forward problems. The time dependent adjoint problems are formulated by perturbing the corresponding Lagrangian functions of the forward problems. Analytical solutions of the adjoint equations at steady state are derived for the 2D Stokes equations and SSA.

Contribution: The work was performed in close collaboration between the authors.

4.5 Paper V

The numerical experiments in this paper are based on the analysis in Paper IV. The adjoint problems are solved backward in time using the solutions from the forward problems. The solutions of the adjoint equations quantify the sensitivity of the parameters to the observations. The weights of the sensitivity are compared with the analytical solutions derived in Paper IV. The estimated perturbations from the sensitivity analysis are in good agreement with those from the numerical experiments of the forward problems.

Contribution: The work was performed in close collaboration between the authors. The author of this thesis performed most of the computations.

4.6 Paper VI

A subgrid model for grounding line migration problem using the Stokes equations is developed within a finite element method. The grounding line position is estimated dynamically in each nonlinear iteration when solving the Stokes equations. The slip boundary conditions are weakly imposed using Nitsche's method and parameterized according to the estimated grounding line position.

This subgrid model is implemented in Elmer/ICE and tested on an advance and a retreat case from the MISMIP benchmark experiments. Comparing to the solutions without subgrid models, similar grounding line migration results are obtained with at least 20 times larger mesh sizes.

Contribution: The author of this thesis implemented the numerical methods and performed the computations. The theory of the paper was developed by the first and second authors. The manuscript was written by all authors.

5. Acknowledgment

First of all, I would like to thank my main supervisor Lina von Sydow for all the support and advise during the past five years. Lina, you have guided me with your passionate leadership and optimistic attitude which are worth learning in my whole life. I am truly grateful that you always encourage me to pursue higher goals and I am proud to be your student.

I would also like to express my heartfelt gratitude to my second supervisor Per Lötstedt for all the great inspirations. Your extensive knowledge is the strongest support to me. I will miss the discussions with you during the fika, in the corridor, in your and my offices.

I am grateful to my co-supervisor Nina Kirchner for providing such an extraordinary ‘FROZEN’ project and supporting me with all the computational resources I need. Your comments on the research projects from the glaciological point of view have broadened my horizon in the interdisciplinary fields.

Special thanks to my ‘academic sister’ Josefin Ahlkrona, following your steps, I see a more clear path to arrive at this point and to continue in academia. Eef van Dongen, your passion to life and the desire for knowledge inspired me. Many thanks to Sergey Marchenkof, your curiosity and ambitious is the key of our successful collaboration. I am grateful to Thomas Zwinger, Peter Råback and the whole Elmer team at CSC-IT Center for Science, Finland, for organizing my visit in January 2017, helping me with all the questions in using and developing Elmer/ICE. I would also like to thank all my co-authors.

I am grateful to all the colleagues at TDB for creating such a great working environment. I would like to thank Adrien Coulier for being the best office-mate, Jonatan Werpens and Slobodan Milovanović for sharing hotel rooms and hanging out during the conferences, Igor Tominec for all the hard work you did in our ongoing project, and Mallin Källén for your valuable help on translating the Swedish summary.

This work was supported by Swedish Research Council FORMAS grant 2013-1600 and 2017-00665 to Nina Kirchner. The computations were performed on resources provided by the Swedish National Infrastructure for Computing (SNIC) at the PDC Center for High Performance Computing, KTH Royal Institute of Technology and through Uppsala Multidisciplinary Center for Advanced Computational Science. I would also like to acknowledge the funding I got for traveling: Liljewalch travel scholarships, Åforsk travel grant, Sederholm-Nordic travel scholarship and SIAM Student Travel Award.

I would like to thank my parents, without your encouragement I would never consider to pursue a PhD abroad. Finally, thank you Jacqueline for making me a better person.

6. Summary in Swedish

Inlandsisar har stor inverkan på klimatet. Numeriska simuleringar ger ett matematiskt verktyg för att studera isarnas historiska rörelser och förutsäga deras framtida bidrag till klimatförändringar. Stora inlandsisar uppför sig som en inkompressibel icke-Newtonsk vätska. Isarnas utveckling styrs av konserveringslagar för massa, rörelsemängd och energi, som formuleras som ett system av partiella differentialekvationer. Eftersom många tillämpningar involverar stora geografiska områden under långa tidsspann, är det önskvärt att förbättra effektiviteten i numeriska simuleringar av inlandsisar. Med detta som mål fokuserar den ena delen av denna avhandling på att utveckla effektiva och noggranna numeriska metoder för simulering av inlandsis.

Flera olika fysikaliska processer är involverade i isens rörelser, som beskrivs av fysikaliska lagar med parametrar uppmätta i experiment och under fältarbete. Dessa parametrar betraktas som input till inlandsissimuleringarna. Under vissa omständigheter är några av dessa parametrar inte kända och kan inte mätas direkt. Därför ägnas den andra delen av denna avhandling åt att hitta dessa fysikaliska parametrar genom att lösa inversa problem.

I den första delen behandlas förbättringar av diskretiseringsmetoder i rum och tid, samt en subgridmodell. Vi utvecklar en adaptiv tidsstegningsmetod i artikel I för att automatiskt justera tidstegen baserat på stabilitets- och noggrannhetskriterier. I artikel II introducerar vi en anisotropisk metod för radiella basfunktioner för rumslig diskretisering av inlandsis i kontinental skala. Vi utformar en subgridmetod för att lösa problem involverande jordningslinjens rörelse med Stokes ekvationer i artikel VI.

Den andra delen av avhandlingen består av analys av och numeriska experiment på inversa problem. I artikel IV och V genomför vi känslighetsanalys och presenterar numeriska exempel på inversa tidsberoende simuleringar av inlandsis. I artikel III löser vi ett inverst problem för värmeledningsförmågan hos firn vid Lomonosovfonna, Svalbard, med hjälp av temperaturmätningar.

References

- [1] J. Ahlkrona, N. Kirchner, and P. Lötstedt. Accuracy of the zeroth- and second-order shallow-ice approximation—numerical and theoretical results. *Geoscientific Model Development*, 6(6):2135–2152, 2013.
- [2] J. Ahlkrona, N. Kirchner, and P. Lötstedt. A numerical study of scaling relations for non-newtonian thin film flows with applications in ice sheet modelling. *The Quarterly Journal of Mechanics and Applied Mathematics*, 66:417–435, 2013.
- [3] J. Ahlkrona, P. Lötstedt, N. Kirchner, and T. Zwinger. Dynamically coupling the non-linear Stokes equations with the shallow ice approximation in glaciology: Description and first applications of the ISCAL method. *Journal of Computational Physics*, 308:1–19, 2016.
- [4] J. Ahlkrona and V. Shcherbakov. A meshfree approach to non-newtonian free surface ice flow: Application to the Haut Glacier d’Arolla. *Journal of Computational Physics*, 330:633–649, 2017.
- [5] R. J. Arthern and G. H. Gudmundsson. Initialization of ice-sheet forecasts viewed as an inverse robin problem. *Journal of Glaciology*, 56(197):527–533, 2010.
- [6] A. Aschwanden, M. A. Fahnestock, M. Truffer, D. J. Brinkerhoff, R. Hock, C. Khroulev, R. Mottram, and S. A. Khan. Contribution of the greenland ice sheet to sea level over the next millennium. *Science advances*, 5(6):eaav9396, 2019.
- [7] H. Blatter. Velocity and stress fields in grounded glaciers: a simple algorithm for including deviatoric stress gradients. *Journal of Glaciology*, 41:333–344, 1995.
- [8] F. Brezzi. On the existence, uniqueness and approximation of saddle-point problems arising from lagrangian multipliers. *Publications mathématiques et informatique de Rennes*, (S4):1–26, 1974.
- [9] F. Brezzi and M. Fortin. *Mixed and hybrid finite element methods*, volume 15. Springer Science & Business Media, 2012.
- [10] D. J. Brinkerhoff and J. Johnson. Data assimilation and prognostic whole ice sheet modelling with the variationally derived, higher order, open source, and fully parallel ice sheet model VarGlaS. *The Cryosphere*, 7:1161, 2013.
- [11] J. Brondex, O. Gagliardini, F. Gillet-Chaulet, and G. Durand. Sensitivity of grounding line dynamics to the choice of the friction law. *Journal of Glaciology*, 63:854–866, 2017.
- [12] E. Bueler and J. Brown. Shallow shelf approximation as a "sliding law" in a thermomechanically coupled ice sheet model. *Journal of Geophysical Research: Earth Surface*, 114(F3), 2009.
- [13] Q. Chen, M. Gunzburger, and M. Perego. Well-posedness results for a nonlinear stokes problem arising in glaciology. *SIAM Journal on Mathematical Analysis*, 45(5):2710–2733, 2013.

- [14] A.-D. Cheng, M. Golberg, E. Kansa, and G. Zammito. Exponential convergence and H-c multiquadric collocation method for partial differential equations. *Numerical Methods for Partial Differential Equations: An International Journal*, 19(5):571–594, 2003.
- [15] F. Chouly, M. Fabre, P. Hild, R. Mlika, J. Pousin, and Y. Renard. An overview of recent results on Nitsche’s method for contact problems. In *Geometrically unfitted finite element methods and applications*, pages 93–141. Springer, 2017.
- [16] F. Chouly, P. Hild, V. Lleras, and Y. Renard. Nitsche-based finite element method for contact with Coulomb friction. In *European Conference on Numerical Mathematics and Advanced Applications*, pages 839–847. Springer, 2017.
- [17] S. Cornford, D. Martin, V. Lee, A. Payne, and E. Ng. Adaptive mesh refinement versus subgrid friction interpolation in simulations of Antarctic ice dynamics. *Annals of Glaciology*, 57:1–9, 2016.
- [18] S. L. Cornford, D. F. Martin, D. T. Graves, D. F. Ranken, A. M. L. Brocq, R. M. Gladstone, A. J. Payne, E. G. Ng, and W. H. Lipscomb. Adaptive mesh, finite volume modeling of marine ice sheets. *Journal of Computational Physics*, 232:529–549, 2013.
- [19] R. M. DeConto and D. Pollard. Contribution of Antarctica to past and future sea-level rise. *Nature*, 531:591–597, 2016.
- [20] E. C. van Dongen, N. Kirchner, M. B. van Gijzen, R. S. van De Wal, T. Zwinger, G. Cheng, P. Lötstedt, and L. von Sydow. Dynamically coupling full Stokes and shallow shelf approximation for marine ice sheet flow using Elmer/ICE (v8. 3). *Geoscientific Model Development*, 11(11):4563–4576, 2018.
- [21] J. K. Dukowicz, S. F. Price, and W. H. Lipscomb. Consistent approximations and boundary conditions for ice-sheet dynamics from a principle of least action. *Journal of Glaciology*, 56:480–496, 2010.
- [22] G. Durand, O. Gagliardini, B. de Fleurian, T. Zwinger, and E. Le Meur. Marine ice sheet dynamics: Hysteresis and neutral equilibrium. *Journal of Geophysical Research: Earth Surface*, 114:F03009, 2009.
- [23] G. Durand, O. Gagliardini, T. Zwinger, E. Le Meur, and R. C. A. Hindmarsh. Full Stokes modeling of marine ice sheets: influence of the grid size. *Annals of Glaciology*, 50:109–114, 2009.
- [24] G. E. Fasshauer. *Meshfree approximation methods with MATLAB*, volume 6. World Scientific, 2007.
- [25] L. P. Franca and S. L. Frey. Stabilized finite element methods: II. The incompressible Navier-Stokes equations. *Computer Methods in Applied Mechanics and Engineering*, 99(2-3):209–233, 1992.
- [26] J. Freund and R. Stenberg. On weakly imposed boundary conditions for second order problems. In *Proceedings of the ninth International Conference on Finite Elements in Fluids*, pages 327–336. Venice, 1995.
- [27] J. Fürst, G. Durand, F. Gillet-Chaulet, N. Merino, L. Tavaré, J. Mouginot, N. Gourmelen, and O. Gagliardini. Assimilation of Antarctic velocity observations provides evidence for uncharted pinning points. *The Cryosphere*, 9(4):1427–1443, 2015.

- [28] O. Gagliardini, J. Brondeur, F. Gillet-Chaulet, L. Tavaré, V. Peyaud, and G. Durand. Impact of mesh resolution for MISMIP and MISMIP3d experiments using Elmer/ICE. *The Cryosphere*, 10(1):307–312, 2016.
- [29] O. Gagliardini, D. Cohen, P. Råback, and T. Zwinger. Finite-element modeling of subglacial cavities and related friction law. *Journal of Geophysical Research: Earth Surface*, 112(F2), 2007.
- [30] O. Gagliardini, T. Zwinger, F. Gillet-Chaulet, G. Durand, L. Favier, B. de Fleurian, R. Greve, M. Malinen, C. Martín, P. Råback, J. Ruokolainen, M. Sacchetti, M. Schäfer, H. Seddik, and J. Thies. Capabilities and performance of Elmer/Ice, a new generation ice-sheet model. *Geoscientific Model Development*, 6:1299–1318, 2013.
- [31] F. Gillet-Chaulet, G. Durand, O. Gagliardini, C. Mosbeux, J. Mouginot, F. Rémy, and C. Ritz. Assimilation of surface velocities acquired between 1996 and 2010 to constrain the form of the basal friction law under pine island glacier. *Geophysical Research Letters*, 43(19):10–311, 2016.
- [32] R. M. Gladstone, R. C. Warner, B. K. Galton-Fenzi, O. Gagliardini, T. Zwinger, and R. Greve. Marine ice sheet model performance depends on basal sliding physics and sub-shelf melting. *The Cryosphere*, 11:319–329, 2017.
- [33] J. W. Glen. The creep of polycrystalline ice. *Proceedings of the Royal Society of London. Series A. Mathematical and Physical Sciences*, 228(1175):519–538, 1955.
- [34] D. Goldberg and P. Heimbach. Parameter and state estimation with a time-dependent adjoint marine ice sheet model. *The Cryosphere*, 7(6):1659–1678, nov 2013.
- [35] D. Goldberg and O. Sergienko. Data assimilation using a hybrid ice flow model. *The Cryosphere*, 5(2):315–327, apr 2011.
- [36] D. N. Goldberg. A variationally derived, depth-integrated approximation to a higher-order glaciological flow model. *Journal of Glaciology*, 57(201):157–170, 2011.
- [37] N. R. Golledge, E. D. Keller, N. Gomez, K. A. Naughten, J. Bernal, L. D. Trusel, and T. L. Edwards. Global environmental consequences of twenty-first-century ice-sheet melt. *Nature*, 566(7742):65, 2019.
- [38] R. Greve and H. Blatter. *Dynamics of Ice Sheets and Glaciers*. Advances in Geophysical and Environmental Mechanics and Mathematics (AGEM²), Springer, Berlin, 2009.
- [39] R. Greve and H. Blatter. Comparison of thermodynamics solvers in the polythermal ice sheet model sicopolis. *Polar Science*, 10(1):11–23, 2016.
- [40] D. F. Griffiths and D. J. Higham. *Numerical methods for ordinary differential equations: initial value problems*. Springer Science & Business Media, 2010.
- [41] I. Griva, S. G. Nash, and A. Sofer. *Linear and nonlinear optimization*, volume 108. SIAM, 2009.
- [42] G. H. Gudmundsson and M. Raymond. On the limit to resolution and information on basal properties obtainable from surface data on ice streams. *The Cryosphere*, 2:167–178, 2008.
- [43] C. Helanow and J. Ahlkrona. Stabilized equal low-order finite elements in ice sheet modeling—accuracy and robustness. *Computational Geosciences*,

- 22(4):951–974, 2018.
- [44] M. J. Hoffman, M. Perego, S. F. Price, W. H. Lipscomb, T. Zhang, D. Jacobsen, I. Tezaur, A. G. Salinger, R. Tuminaro, and L. Bertagna. MPAS-Albany Land Ice (MALI): a variable-resolution ice sheet model for Earth system modeling using Voronoi grids. *Geoscientific Model Development*, 11(9):3747–3780, 2018.
- [45] K. Hutter. *Theoretical Glaciology*. D. Reidel Publishing Company, Terra Scientific Publishing Company, Dordrecht, 1983.
- [46] P. Huybrechts, A. J. Payne, and the EISMINT intercomparison group. The EISMINT benchmarks for testing ice sheet models. *Annals of Glaciology*, 23:1–12, 1996.
- [47] T. Isaac, N. Petra, G. Stadler, and O. Ghattas. Scalable and efficient algorithms for the propagation of uncertainty from data through inference to prediction for large-scale problems with application to flow of the Antarctic ice sheet. *Journal of Computational Physics*, 296:348–368, 2015.
- [48] T. Isaac, G. Stadler, and O. Ghattas. Solution of nonlinear Stokes equations discretized by high-order finite elements on nonconforming and anisotropic meshes, with application to ice sheet dynamics. *SIAM Journal on Scientific Computing*, 37(6):B804–B833, 2015.
- [49] M. Jay-Allemand, F. Gillet-Chaulet, O. Gagliardini, and M. Nodet. Investigating changes in basal conditions of Variegated Glacier prior to and during its 1982-1983 surge. *The Cryosphere*, 5:659–672, 2011.
- [50] E. J. Kansa. Multiquadrics—a scattered data approximation scheme with applications to computational fluid-dynamics—I surface approximations and partial derivative estimates. *Computers & Mathematics with applications*, 19(8-9):127–145, 1990.
- [51] E. J. Kansa. Multiquadrics—a scattered data approximation scheme with applications to computational fluid-dynamics—II solutions to parabolic, hyperbolic and elliptic partial differential equations. *Computers & mathematics with applications*, 19(8-9):147–161, 1990.
- [52] N. Kirchner, J. Ahlkrone, E. Gowan, P. Lötstedt, J. Lea, R. Noormets, L. von Sydow, J. Dowdeswell, and T. Benham. Shallow ice approximation, second order shallow ice approximation, and full Stokes models: A discussion of their roles in palaeo-ice sheet modelling and development. *Quaternary Science Reviews*, 135:103 – 114, 2016.
- [53] R. Lamour, R. März, and C. Tischendorf. *Differential-algebraic equations: a projector based analysis*. Springer Science & Business Media, 2013.
- [54] E. Larour, H. Seroussi, S. Adhikari, E. Ivins, L. Caron, M. Morlighem, and N. Schlegel. Slowdown in Antarctic mass loss from solid earth and sea-level feedbacks. *Science*, 364:eaav7908, 2019.
- [55] E. Larour, H. Seroussi, M. Morlighem, and E. Rignot. Continental scale, high order, high spatial resolution, ice sheet modeling using the Ice Sheet System Model (ISSM). *Journal of Geophysical Research: Earth Surface*, 117:F01022, 2012.
- [56] M. G. Larson and F. Bengzon. *The finite element method: theory, implementation, and applications*, volume 10. Springer Science & Business Media, 2013.

- [57] W. Leng, L. Ju, M. Gunzburger, S. Price, and T. Ringler. A parallel high-order accurate finite element nonlinear Stokes ice sheet model and benchmark experiments. *Journal of Geophysical Research: Earth Surface*, 117:2156–2202, 2012.
- [58] P. Lötstedt, S. Söderberg, A. Ramage, and L. Hemmingsson-Frändén. Implicit solution of hyperbolic equations with space-time adaptivity. *BIT Numerical Mathematics*, 42(1):134–158, 2002.
- [59] D. R. MacAyeal. Large-scale ice flow over a viscous basal sediment: Theory and application to Ice Stream B, Antarctica. *Journal of Geophysical Research*, 94:4071–4078, 1989.
- [60] D. R. MacAyeal. The basal stress distribution of Ice Stream E, Antarctica, inferred by control methods. *Journal of Geophysical Research*, 97:595–603, 1992.
- [61] D. R. MacAyeal. A tutorial on the use of control methods in ice sheet modeling. *Journal of Glaciology*, 39:91–98, 1993.
- [62] N. Martin and J. Monnier. Four-field finite element solver and sensitivities for quasi-newtonian flows. *SIAM Journal on Scientific Computing*, 36(5):S132–S165, 2014.
- [63] J. H. Mercer. West Antarctic ice sheet and CO₂ greenhouse effect: a threat of disaster. *Nature*, 271(5643):321, 1978.
- [64] B. Minchew, M. Simons, H. Björnsson, F. Pálsson, M. Morlighem, H. Seroussi, E. Larour, and S. Hensley. Plastic bed beneath Hofsjökull Ice Cap, central Iceland, and the sensitivity of ice flow to surface meltwater flux. *Journal of Glaciology*, 62:147–158, 2016.
- [65] B. M. Minchew, C. R. Meyer, S. S. Pegler, B. P. Lipovsky, A. W. Rempel, G. H. Gudmundsson, and N. R. Iverson. Comment on "Friction at the bed does not control fast glacier flow". *Science*, 363:eaau6055, 2019.
- [66] L. Morland. Unconfined ice-shelf flow. In *Dynamics of the West Antarctic Ice Sheet*, pages 99–116. Springer, 1987.
- [67] L. W. Morland. Thermo–mechanical balances of ice sheet flows. *Geophysical & Astrophysical Fluid Dynamics*, 29:237–266, 1984.
- [68] M. Morlighem, E. Rignot, H. Seroussi, E. Larour, H. Ben Dhia, and D. Aubry. Spatial patterns of basal drag inferred using control methods from a full-Stokes and simpler models for Pine Island Glacier, West Antarctica. *Geophysical Research Letters*, 37(14), 2010.
- [69] C. Mosbeux, F. Gillet-Chaulet, and O. Gagliardini. Comparison of adjoint and nudging methods to initialise ice sheet model basal conditions. *Geoscientific Model Development*, 9:2549–2562, 2016.
- [70] J. Nitsche. Über ein Variationsprinzip zur Lösung von Dirichlet-Problemen bei Verwendung von Teilräumen, die keinen Randbedingungen unterworfen sind. *Abh. Math. Semin., University of Hamburg, Germany*, 36:9–15, 1971.
- [71] J. Nye. The motion of ice sheets and glaciers. *Journal of Glaciology*, 3(26):493–507, 1959.
- [72] F. Pattyn. A new three-dimensional higher-order thermomechanical ice sheet model: Basic sensitivity, ice stream development, and ice flow across subglacial lakes. *Journal of Geophysical Research*, 108:2382, 2003.
- [73] F. Pattyn. The paradigm shift in Antarctic ice sheet modelling. *Nature*

- communications*, 9(1):2728, 2018.
- [74] F. Pattyn, A. Huyghe, S. De Brabander, and B. De Smedt. Role of transition zones in marine ice sheet dynamics. *Journal of Geophysical Research: Earth Surface*, 111(F2), 2006.
- [75] F. Pattyn, L. Perichon, A. Aschwanden, B. Breuer, B. de Smedt, O. Gagliardini, G. H. Gudmundsson, R. Hindmarsh, A. Hubbard, J. V. Johnson, T. Kleiner, Y. Konovalov, C. Martin, A. J. Payne, D. Pollard, S. Price, M. Rückamp, F. Saito, O. Souček, S. Sugiyama, and T. Zwinger. Benchmark experiments for higher-order and full-Stokes ice sheet models (ISMIP-HOM). *The Cryosphere*, 2:95–108, 2008.
- [76] F. Pattyn, L. Perichon, G. Durand, L. Favier, O. Gagliardini, R. C. A. Hindmarsh, T. Zwinger, T. Albrecht, S. Cornford, D. Docquier, J. J. Fürst, D. Goldberg, G. H. Gudmundsson, A. Humbert, M. Hütten, G. Jouvét, T. Kleiner, E. Larour, D. Martin, M. Morlighem, A. J. Payne, D. Pollard, M. Rückamp, O. Rybak, H. Seroussi, M. Thoma, and N. Wilkens. Grounding-line migration in plan-view marine ice-sheet models: results of the ice2sea MISMIP3d intercomparison. *Journal of Glaciology*, 59:410–422, 2013.
- [77] F. Pattyn, C. Schoof, L. Perichon, R. C. A. Hindmarsh, E. Bueller, B. de Fleurian, G. Durand, O. Gagliardini, R. Gladstone, D. Goldberg, G. H. Gudmundsson, P. Huybrechts, V. Lee, F. M. Nick, A. J. Payne, D. Pollard, O. Rybak, F. Saito, and A. Vieli. Results of the Marine Ice Sheet Model Intercomparison Project, MISMIP. *The Cryosphere*, 6:573–588, 2012.
- [78] A. J. Payne, P. Huybrechts, A. Abe-Ouchi, R. Calov, J. L. Fastook, R. Greve, S. J. Marshall, I. Marsiat, C. Ritz, L. Tarasov, and M. P. A. Thomassen. Results from the EISMINT model intercomparison: the effects of thermomechanical coupling. *Journal of Glaciology*, 46:227–238, 2000.
- [79] M. Perego, M. Gunzburger, and J. Burkardt. Parallel finite-element implementation for higher-order ice-sheet models. *Journal of Glaciology*, 58(207):76–88, 2012.
- [80] N. Petra, J. Martin, G. Stadler, and O. Ghattas. A computational framework for infinite-dimensional Bayesian inverse problems, Part II: Newton MCMC with application to ice sheet flow inverse problems. *SIAM Journal on Scientific Computing*, 36:A1525–A1555, 2014.
- [81] N. Petra, H. Zhu, G. Stadler, T. J. R. Hughes, and O. Ghattas. An inexact Gauss-Newton method for inversion of basal sliding and rheology parameters in a nonlinear Stokes ice sheet model. *Journal of Glaciology*, 58:889–903, 2012.
- [82] D. Pollard and R. DeConto. Description of a hybrid ice sheet-shelf model, and application to Antarctica. *Geoscientific Model Development*, 5(5):1273–1295, 2012.
- [83] D. Pollard and R. M. DeConto. Modelling West Antarctic ice sheet growth and collapse through the past five million years. *Nature*, 458:329–332, 2009.
- [84] M. J. Raymond and H. Gudmundsson. Estimating basal properties of ice streams from surface measurements: a non-linear Bayesian inverse approach applied to synthetic data. *The Cryosphere*, 3(2):265–278, 2009.
- [85] F. Riche and M. Schneebeli. Thermal conductivity of snow measured by three

- independent methods and anisotropy considerations. *The Cryosphere*, 7(1):217–227, 2013.
- [86] C. Ritz, T. L. Edwards, G. Durand, A. J. Payne, V. Peyaud, and R. C. Hindmarsh. Potential sea level rise from Antarctic ice-sheet instability constrained by observations. *Nature*, 528:115–118, 2015.
- [87] C. Schoof. The effect of cavitation on glacier sliding. *Proceedings of the Royal Society A: Mathematical, Physical and Engineering Sciences*, 461(2055):609–627, 2005.
- [88] C. Schoof. Ice sheet grounding line dynamics: Steady states, stability and hysteresis. *Journal of Geophysical Research: Earth Surface*, 112:F03S28, 2007.
- [89] C. Schoof. Marine ice-sheet dynamics. Part 1. The case of rapid sliding. *Journal of Fluid Mechanics*, 573:27–55, 2007.
- [90] C. Schoof. Marine ice sheet dynamics. Part 2. A Stokes flow contact problem. *Journal of Fluid Mechanics*, 679:122–155, 2011.
- [91] C. Schoof and R. Hindmarsh. Thin-film flows with wall slip: An asymptotic analysis of higher order glacier flow models. *The Quarterly Journal of Mechanics and Applied Mathematics*, 63:73–114, 2010.
- [92] H. Seddik, R. Greve, T. Zwinger, F. Gillet-Chaulet, and O. Gagliardini. Simulations of the Greenland ice sheet 100 years into the future with the full Stokes model Elmer/Ice. *Journal of Glaciology*, 58:427–440, 2012.
- [93] O. V. Sergienko, D. R. MacAyeal, and J. E. Thom. Reconstruction of snow/firn thermal diffusivities from observed temperature variation: application to iceberg C16, ross sea, Antarctica, 2004–07. *Annals of Glaciology*, 49:91–95, 2008.
- [94] H. Seroussi and M. Morlighem. Representation of basal melting at the grounding line in ice flow models. *The Cryosphere*, 12(10):3085–3096, 2018.
- [95] H. Seroussi, M. Morlighem, E. Larour, E. Rignot, and A. Khazendar. Hydrostatic grounding line parameterization in ice sheet models. *The Cryosphere*, 8:2075–2087, 2014.
- [96] H. Seroussi, S. Nowicki, E. Simon, A. Abe-Ouchi, T. Albrecht, J. Brondex, S. Cornford, C. Dumas, F. Gillet-Chaulet, H. Goelzer, et al. initMIP-Antarctica: an ice sheet model initialization experiment of ISMIP6. *The Cryosphere*, 13(5):1441–1471, 2019.
- [97] R. C. Smith. *Uncertainty Quantification. Theory, Implementation, and Applications*. Society for Industrial and Applied Mathematics, Philadelphia, 2014.
- [98] G. Söderlind and L. Wang. Adaptive time-stepping and computational stability. *Journal of Computational and Applied Mathematics*, 185(2):225–243, 2006.
- [99] A. J. Sole, D. W. F. Mair, P. W. Nienow, I. D. Bartholomew, I. D. King, M. A. Burke, and I. Joughin. Seasonal speedup of a Greenland marine-terminating outlet glacier forced by surface melt-induced changes in subglacial hydrology. *Journal of Geophysical Research*, 116:F03014, 2011.
- [100] L. A. Stearn and C. J. van der Veen. Friction at the bed does not control fast glacier flow. *Science*, 361:273–277, 2018.
- [101] C. R. Stokes, L. Tarasov, R. Blomdin, T. M. Cronin, T. G. Fisher, R. Gyllencreutz, C. Hättestrand, J. Heyman, R. C. Hindmarsh, A. L. Hughes,

- et al. On the reconstruction of palaeo-ice sheets: recent advances and future challenges. *Quaternary Science Reviews*, 125:15–49, 2015.
- [102] I. K. Tezaur, M. Perego, A. G. Salinger, R. S. Tuminaro, and S. F. Price. Albany/FELIX: a parallel, scalable and robust, finite element, first-order Stokes approximation ice sheet solver built for advanced analysis. *Geoscientific Model Development*, 8:1197–1220, 2015.
- [103] I. K. Tezaur, R. S. Tuminaro, M. Perego, A. G. Salinger, and S. F. Price. On the scalability of the Albany/FELIX first-order Stokes approximation ice sheet solver for large-scale simulations of the Greenland and Antarctic ice sheets. *Procedia Computer Science*, 51:2026–2035, 2015.
- [104] V. C. Tsai, A. L. Stewart, and A. F. Thompson. Marine ice-sheet profiles and stability under coulomb basal conditions. *Journal of Glaciology*, 61(226):205–215, 2015.
- [105] R. Tuminaro, M. Perego, I. Tezaur, A. Salinger, and S. Price. A matrix dependent/alebraic multigrid approach for extruded meshes with applications to ice sheet modeling. *SIAM Journal on Scientific Computing*, 38(5):C504–C532, 2016.
- [106] D. G. Vaughan and R. Arthern. Why is it hard to predict the future of ice sheets? *Science*, 315:1503–1504, 2007.
- [107] A. Vieli, A. J. Payne, Z. Du, and A. Shepherd. Numerical modelling and data assimilation of the larsen b ice shelf, Antarctic peninsula. *Philosophical Transactions of the Royal Society A: Mathematical, Physical and Engineering Sciences*, 364(1844):1815–1839, 2006.
- [108] J. Weertman. On the sliding of glaciers. *Journal of Glaciology*, 3:33–38, 1957.
- [109] H. Wendland. Fast evaluation of radial basis functions: Methods based on partition of unity. In *Approximation theory X: wavelets, splines, and applications*. Citeseer, 2002.
- [110] R. Winkelmann, M. A. Martin, M. Haseloff, T. Albrecht, E. Bueler, C. Khroulev, and A. Levermann. The Potsdam parallel ice sheet model (PISM-PIK)—Part 1: Model description. *The Cryosphere*, 5(3):715–726, 2011.
- [111] H. Yu, E. Rignot, H. Seroussi, and M. Morlighem. Retreat of Thwaites Glacier, West Antarctica, over the next 100 years using various ice flow models, ice shelf melt scenarios and basal friction laws. *The Cryosphere*, 12:3861–3876, 2018.
- [112] T. Zhang, S. Price, L. Ju, W. Lei, J. Brondex, G. Durand, and O. Gagliardini. A comparison of two Stokes ice sheet models applied to the Marine Ice Sheet Model Intercomparison Project for plan view models. *The Cryosphere*, 11:179–190, 2017.
- [113] T. Zwinger, R. Greve, O. Gagliardini, T. Shiraiwa, and M. Lyly. A full Stokes-flow thermomechanical model for firn and ice applied to the Gorshkov crater glacier, Kamchatka. *Annals of Glaciology*, 45:29–37, 2007.

Acta Universitatis Upsaliensis

*Digital Comprehensive Summaries of Uppsala Dissertations
from the Faculty of Science and Technology 1849*

Editor: The Dean of the Faculty of Science and Technology

A doctoral dissertation from the Faculty of Science and Technology, Uppsala University, is usually a summary of a number of papers. A few copies of the complete dissertation are kept at major Swedish research libraries, while the summary alone is distributed internationally through the series Digital Comprehensive Summaries of Uppsala Dissertations from the Faculty of Science and Technology. (Prior to January, 2005, the series was published under the title “Comprehensive Summaries of Uppsala Dissertations from the Faculty of Science and Technology”.)

Distribution: publications.uu.se
urn:nbn:se:uu:diva-392268



ACTA
UNIVERSITATIS
UPSALIENSIS
UPPSALA
2019